Int. J. Electrochem. Sci., 17 **(2022)** Article Number: 220736, doi: 10.20964/2022.07.37

International Journal of
ELECTROCHEMICAL
SCIENCE
www.electrochemsci.org

A Novel Molecularly Imprinted Membrane for Highly Sensitive Electrochemical Detection of Paracetamol

Bingxin Zheng[1,2], *Xiaowen He*[1,2], *Qiu Zhang*[1,2], *Mengting Duan*[1,2*]

[1] Department of Pharmacy, The First Hospital of China Medical University, No.155 Nnajing Street, Heping District, Shenyang 110000, China
[2] School of Pharmacy, China Medical University, Shenyang, Liaoning Province, 110001, China
[*]E-mail: duanmengting123@126.com

Received: 24 March 2022 / *Accepted:* 5 May 2022 / *Published:* 6 June 2022

Molecularly imprinted polymers (MIPs) have been widely used for sensor fabrication. Paracetamol (PA) is a frequently prescribed antipyretic. With MIP and membrane separation technologies, a MIP was successfully synthesized in this study with PA being the template molecule. MIP was adopted to modify the electrodes in order to increase the sensitivity of the PA detection. The blotting, elution, and electrode regeneration mechanisms were also discussed and the adsorption of PA onto the electrode was investigated. The MIP-based electrochemical sensor can detect PA linearly from 1 pM to 0.1 mM with a detection limit of 3.6 pM under ideal conditions. In addition, the proposed sensor showed an excellent anti-interference performance.

Keywords: Electrochemical sensor; Paracetamol; Molecularly imprinted polymers; Glucose; Uric acid

1. INTRODUCTION

Paracetamol (PA) is commonly used acetanilide antipyretic analgesic drugs. It was first synthesized by Morse in 1878 and first applied in clinical practice by Von Mering in 1893. However, it was not marketed as a drug until it was identified as an active metabolite of phenacetin and acetaniline in 1948. With more than 100 years of development, PA has been widely used and has become an important antipyretic analgesic in the international pharmaceutical market [1,2]. PA is a white or quasi-white crystalline or crystalline powder whose antipyretic action is similar to aspirin. Its analgesic effect is weak, without anti-inflammatory and anti-rheumatism effect, and it is the best variety of acetanilide drugs, especially suitable for patients who cannot use carboxylic acid drugs [3,4]. PA has been increasingly applied as a substitute for phenacetin, for the reason that it has fewer side effects than phenacetin. It is generally used in clinical treatment of cold and fever, headache, analgesia after operation [5]. Since the first report of severe liver damage resulted from excessive use of PA in 1966, people have

started to attach importance to the study of its toxicity. In recent years, PA has been reported as a risk factor for asthma, allergic disease and stroke. The FDA's latest prescription combination products with PA contain no more than 325 mg of acetaminophen per capsule [6–9]. These results indicate that accurate detection of PA content in drugs is of great significance for drug quality control and medication safety.

Up to present, a number of methods have been adopted to determine the content of PA in drugs, including spectrophotometry, high performance liquid chromatography, capillary electrophoresis, flow injection chemiluminescence, fluorescence, and electrochemical method [10–14], among which electrochemical method is easy to obtain and operate with low cost and without complex pretreatment, which greatly shortens the detection time. It is a qualitative and quantitative instrumental analysis method based on the measurement relationship between potential, conductance, current, electric quantity and some quantity of the measured substance, as well as the electrochemical properties of the measured substance in solution and its changing rules [15–18]. Electrochemical method has the characteristics of high sensitivity, high accuracy, wide measuring range, easy equipment, simple operation and low cost. The most widely applied electrochemical method for PA determination is material modified electrode [19], which has high sensitivity. However, it has no specific selectivity for acetaminophen [20–25].

Molecularly imprinted membranes have high selectivity and recognition of template molecules. It refers to the process of preparing polymers that are specifically selective for a particular target molecule, and is also graphically described as the "artificial lock" technique for preparing "molecular keys". Molecularly imprinted polymers (MIPs) are such synthetic artificial receptors with a cavity whose shape matches that of the substrate molecule and has a specific arrangement of functional groups that can be recognized by the substrate molecule [26–28]. In this study, PA was used as a template, α-methylphenenic acid (MAA) as a functional monomer, dimethyl sulphoxide (DMSO) as a solvent, ethylene glycol dimethylpropylester (EGDMA) as a crosslinking agent, and azodiethylbutylamine (AIBN) as an initiator. The PA molecularly imprinted polymer was then prepared [29]. The optimal preparation technique was developed after the dose of functional monomer, imprinting mechanism, and micromorphology of imprinted polymer were investigated in the experiment. Through merging molecularly imprinted technology with chemically modified electrode, a molecularly imprinted polymer membrane modified electrode was created [30]. With this approach, an electrode that may be used to determine PA in solution can be produced and has high stability and selectivity.

2. EXPERIMENTAL

PA, MAA, EGDMA, AIBN and DMSO were all purchased from Nanjing Youyun Biotech. Co., Ltd. All of the other reagents were of analytical grade. The electrolyte used for electrochemical sensing was phosphate-buffered saline (PBS).

All electrochemical experiments were conducted with a CHI660E electrochemical workstation. A three-electrodes system was adopted through all measurements, while a glassy carbon electrode (GCE), a Pt wire and an Ag/AgCl (3M KCl) were applied as working electrode, counter electrode and reference electrode, respectively. The UV-vis spectra of samples were recorded by a UV-204 dual-

wavelength UV-visible spectrophotometer (Shimadzu). FTIR spectra were recorded with a TENSOR37(BRUKER) FTIR spectrometer.

0.20 g (1 mM) template molecule PA was weighed and dispersed into 400 mL DMSO. 0.5 mL (2 mM) functional monomer MAA was added into the solution and sonicated at room temperature for 1 h. Different ratios of DMSO with PA+MMA (1:0, 1:1, 1:2, 1:3, 1:4, 1:5 and 1:6) were used for optimization of MIP. Afterwards, a certain amount of crosslinking agent EGDMA and initiator AIBN were added. Nitrogen was injected into solution for 30 min before sealing, after which the solution was placed in a collector constant temperature heating magnetic stirring device at 50°C to initiate the polymerization for 24 h. After being cooled to room temperature, the reactants were centrifuged to obtain imprinted polymer microspheres (MIPs). The synthesized polymer microspheres were put into a Soxhlet extractor and extracted with methanol/acetic acid (V/V = 9/1) to elute the imprinted molecules until PA in the reflux solution could not be detected by UV spectroscopy. It was then washed several times with methanol to remove excess acetic acid, and finally dried in a vacuum oven at 60°C for later use (denoted as MIP(I)). The elution time was optimized during the experiments. 5 μL MIPs solution (1 mg/mL) was coated to the surface of the GCE and dried naturally. Non-imprinted polymer microspheres (NIPs) were synthesized with a similar method without addition of PA.

10 mg of MIP and NIP was weighed respectively, and 5 mL of PA-DMSO solution (2 mM) was added. The solution was sonicated at room temperature for re-identification (0, 10, 20, 30 min). After the re-identification, the mixture at each time was immediately transferred to the separator for centrifugation for 15 min. Afterwards, 1 mL supernatant was diluted with 5 mL DMSO. The absorbance of the solution was measured at the maximum absorption wavelength by an UV spectrophotometer with DMSO being a reference. The equilibrium concentration of template molecule PA was determined.

3. RESULTS AND DISCUSSION

Figure 1 shows a series of UV absorption spectra, and the concentration of the imprinted molecule PA remains stable, but the concentration of the functional monomer MAA grows with time. The absorbance decreases with the increase of the amount of the introduced functional monomers, suggesting that the contact force between the functional monomer MAA and the imprinted molecule PA increases. When the molar ratio of the imprinted molecule to the functional monomer is larger than 1:5, the amount of functional monomer continues to rise, and the change in the intensity of the absorption peak is less noticeable, which illustrates that increasing the fraction of functional monomers can improve self-assembly between imprinted molecules and functional monomers within a particular range [31,32]. The reason for this phenomenon is that a high concentration of functional monomers can cause the formation of unassembled functional monomer residues. As a result, the MIP will have more non-selective binding sites and fewer particular selective recognition sites. Moreover, if the number of functional monomers is too large, self-association is more likely to occur, resulting in incorrect immobilization and the development of identification sites, as well as an increase in the mass transfer resistance of MIP adsorption [33,34]. Therefore, 1:5 was chosen as the ideal molar ratio for the synthesis

of MIP in the experiment in order to increase the recognition efficiency and stability of the generated MIP.

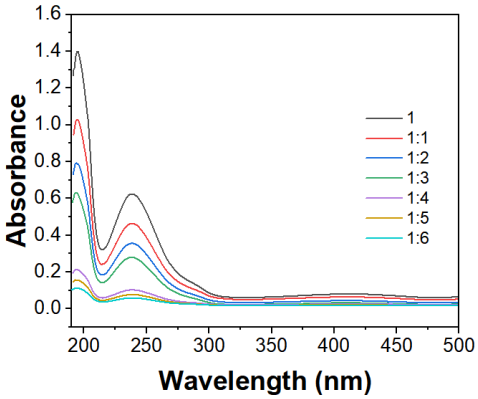

Figure 1. UV-vis spectra of PA and MAA with different rations in DMSO.

The functional groups and chemical bonds of the tested compounds may be identified based on the position, intensity, and shape of the absorption peaks in the infrared spectrum, thus studying the FTIR spectra of each polymer can help researchers learn more about the unique functional groups that interact with functional monomers and the imprinting process of MIP synthesis. The infrared spectra of MIP before elution, target molecule PA, MIP, and NlP after elution are shown in Figure 2. The stretching vibration absorption peak of OH is around 3211cm^{-1} in the infrared spectrum of PA. The stretching vibration absorption peak of aldehyde group is around 1669 cm^{-1}, whereas the bending vibration absorption peak of the phenolic hydroxyl group is around 1255 cm^{-1}.

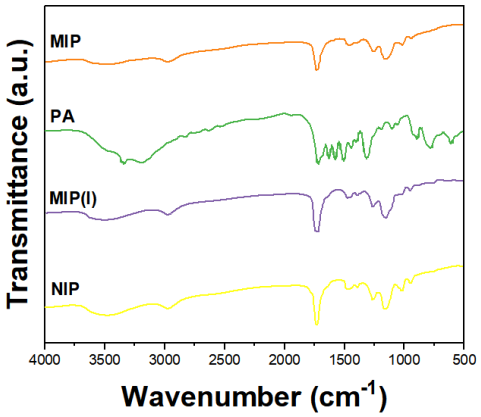

Figure 2. FTIR spectra of MIP, PA, MIP after elution and NIP.

The stretching vibration absorption peak band of the original template molecule PA at 1666 cm^{-1} moves to roughly 1732 cm^{-1} in the high wavenumber band in the FTIR spectrum of MIP before elution [35]. The C=O bond in the PA molecule may establish a hydrogen bonding site with the ammonia atom on COOH in MAA, implying that the C=O bond in the PA molecule may form a hydrogen bonding site

with the ammonia atom on COOH in MAA. On clean PA, however, the stretching vibration absorption peak of the OH bond, which is around 3202 cm^{-1}, is blue-shifted to around 3400 cm^{-1}. It demonstrates that PA and MAA have a high intermolecular interaction, and it is possible that a strong hydrogen bond exists between -OH in PA and C=O in MAA [36]. Furthermore, the infrared spectral properties of eluted MIP and NIP are almost identical, showing that the template molecule PA in MIP was eluted, leaving a hole structure that matches its functional group [37].

The kinetic adsorption curve, which displays the connection between the adsorption amount Qt (the adsorption amount at a specific time) and the time t, is an essential tool for studying the adsorption kinetics of imprinted polymers. In this study, the adsorption capability of imprinted polymer to target molecules at different periods was investigated under the conditions of constant polymer mass and starting concentration of template molecule solution. The adsorption kinetic curves of MIP and NIP are shown in Figure 3A.

It can be seen from Figure 3A that the adsorption rate accelerates dramatically with time. As a particular amount of time has passed, the growing rate of adsorption slows down, and the adsorption eventually reaches equilibrium. The reason for this phenomenon is the enormous number of holes and cavities on the MIP surface during the first stages of adsorption, which can be congruent with the template's molecular structure [38]. The pores and cavities on these surfaces are used by MIP to identify the adsorbed imprinted molecule PA, therefore the MIP has a greater adsorption rate to the imprinted molecule at this stage. The effective binding sites among the surface pores rapidly diminish as the adsorption process progresses and the rate of adsorption decreases. When the adsorption among these surface pores and cavities becomes saturated, the imprinted molecules begin to diffuse into the MIP's deep pores, resulting in a certain mass transfer resistance. The rate of adsorption decreases until the adsorption equilibrium is attained [39]. Furthermore, MIP's PA adsorption capacity is substantially greater than NIP's PA adsorption capacity at the same period, demonstrating that MIP has a better adsorption capacity for PA. The pseudo-first-order kinetic model and the pseudo-second-order kinetic model can be adopted to describe the adsorption kinetic process [40]. The kinetic adsorption data of the imprinted microspheres were fitted in this study, and their linear correlations were evaluated. The results show that the pseudo-second-order kinetic model can better match the adsorption features of imprinted microspheres (Figure 3B).

In the 5 mM $[Fe(CN)_6]^{3-/4-}$ solution, the electrodes were characterized with two electrochemical measurements: cyclic voltammetry (CV) and EIS. The CV curves of several polymerization phases are shown in Figure 4A. It can be noted that the $[Fe(CN)_6]^{3-/4-}$ probe ions easily undergo redox reactions on the bare electrode surface. The current signal drops after being adjusted by MIP and coupled with PA, the reason for which is that the part of $[Fe(CN)_6]^{3-/4-}$ is prevented from entering the electrode surface by PA covering [41,42]. Following the elution of the template molecule in MIP, $[Fe(CN)_6]^{3-/4-}$ may touch the electrode surface through the imprinted cavity, resulting in an electrochemical reaction and a modest rise in current. After the PA molecules are identified, template molecules fill a portion of the cavities, lowering the number of $[Fe(CN)_6]^{3-/4-}$ reaching the electrode surface and lowering the response current intensity [43].

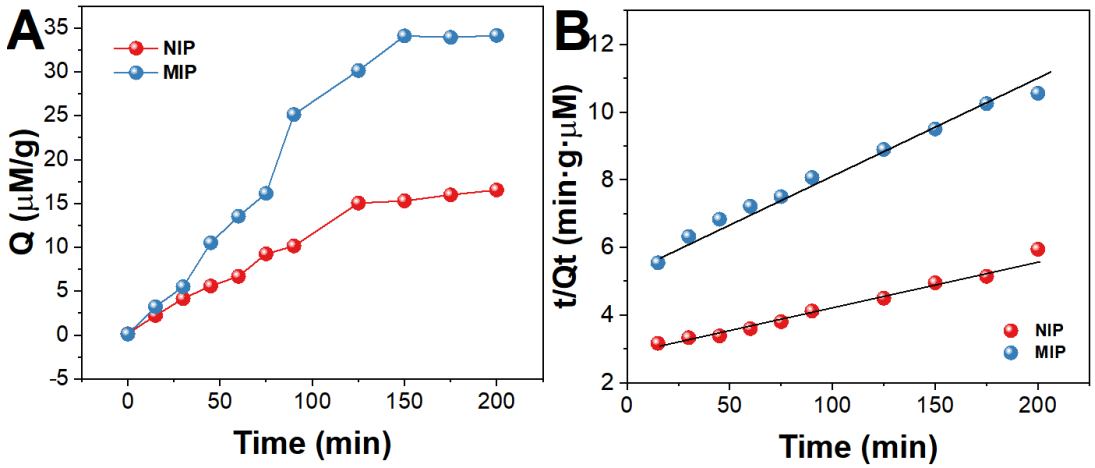

Figure 3. (A) Adsorption dynamic curves and (B) second-order kinetics of MIP and NIP on PA.

In the investigation of charge transport during electrode interface identification, EIS has been frequently employed. In the frequency range of 100 kHz to 0.1 Hz, the EIS of each stage of electrode modification was measured. Rs is the electrolyte resistance, C_{dl} is the interface capacitance, R_{ct} is the charge transfer resistance, and Z_w is the Warburg impedance (Figure 4B). The diameter of the high-frequency semicircle in the spectrogram corresponds to the redox probe's electron transfer resistance R_{ct} [44]. The R_{ct} of the charge transfer resistance increases and the semicircle diameter grows after altering the MIP on the electrode surface and recognizing the PA, which suggests that PA molecules on the electrode surface obstruct the redox probes on the electrode surface. The impedance value falls when the template molecules are rinsed owing to the creation of imprinted molecular cavities on the electrode surface [45]. When the target molecule is identified again, the cavity is filled with PA molecules, and the impedance rises, as in the previous current transformation.

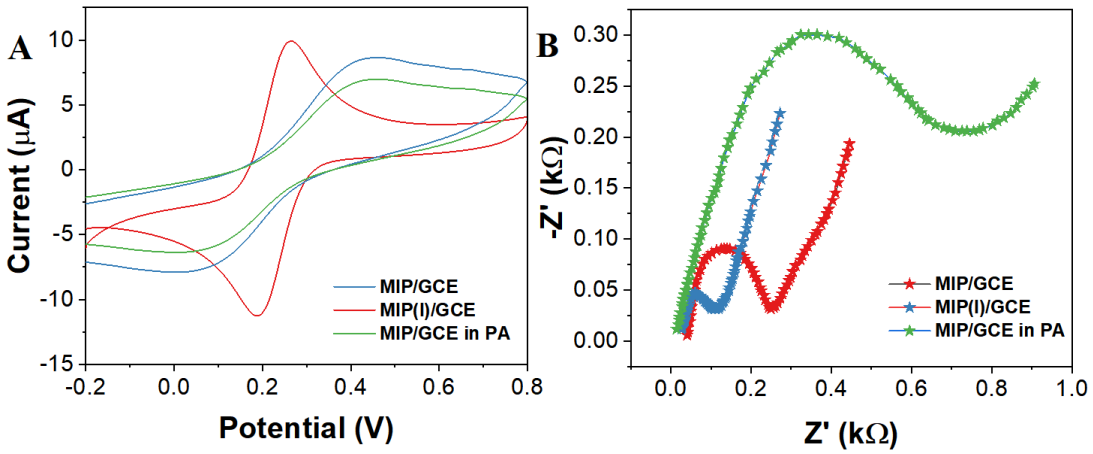

Figure 4. (A) CV and (B) EIS curves of GCE, MIP/GCE, MIP(I)/GCE and MIP/GCE/PA in 5 mM $[Fe(CN)_6]^{3-/4-}$ (CV scan rate: 50 mV/s; EIS frequency range: 100 kHz to 0.1 Hz).

In the study, conditions such as template elution duration and re-identification time were tuned to increase the electrochemical sensor's detection capability. The PA was withdrawn from the MIP to produce a cavity, and the elution duration was adjusted using ethanol/acetic acid (V/V = 95:5) as the eluent. The change in current responsiveness during elution is presented in Figure 5A. The response current value increases with the elution duration, suggesting that the template molecules are gradually eluted and the imprinted cavity grows [46]. Meanwhile, through the cavity, the $[Fe(CN)_6]^{3-/4-}$ electroactive probe reaches the electrode surface, and the response current steadily rises. The peak current and impedance value approach equilibrium and tend to remain steady when the elution duration is 20 min, thus the ideal elution time is 20 min. In the experiment, the electrodes were submerged in water for 10 min and properly cleaned after electrochemical tests to eliminate leftover ethanol, acetic acid, and adsorption matrix.

The time required for re-identification is a critical factor in evaluating the efficacy of electrochemical sensors. Electrodes were placed in 0.2 mM PA to maximize the blot chamber's filling time. After electrodes were identified, they were properly washed with water and electrochemical measurements were made. The changes in the current reaction through the re-identification procedure are depicted in Figure 5B. As seen in the picture, as the re-identification time increases, the peak current value lowers progressively, indicating that the cavity is gradually populated by template molecules [47]. Simultaneously, the number of electrochemically active $[Fe(CN)_6]^{3-/4-}$ probes in contact with the electrode surface steadily reduces. As the imprinted cavity fills with target molecules, the resistance increases progressively. After 20 min of identification, the peak current and impedance attain equilibrium. As a result, the optimal time for re-identification of PA is 20 min. The current value in Figure 5 is the current value of the oxidation peak of $[Fe(CN)_6]^{3-/4-}$ of the MIP sensor combined with the new PA. As the cavity in MIP is filled again with a certain concentration of PA, the electron transfer capacity of the interface changes, resulting in a change in the current value of $[Fe(CN)_6]^{3-/4-}$ redox. However, since the expression of CV was not significantly different visually, we chose EIS as the analysis technique in the follow-up investigation.

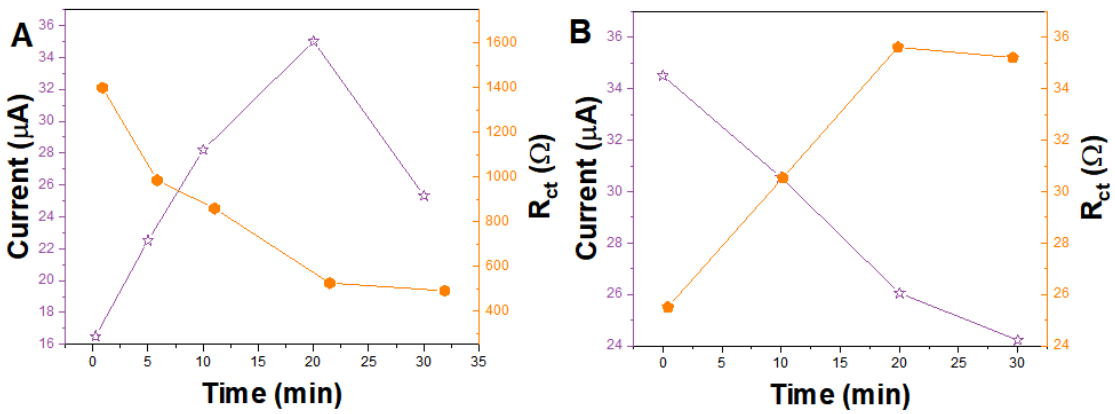

Figure 5. The influence of elution time (A) and re-identification time (B) on the response signal in 5 mM $[Fe(CN)_6]^{3-/4-}$ (scan rate: 50 mV/s).

To determine the response of MIP/GCE towards PA, we recorded electrochemical signals at PA concentrations ranging from 10 pM to 100 µM in PBS under optimum circumstances. After 20 min in PA solution, the EIS curve of MIP/GCE was measured. As illustrated in Figure 6A, charge transfer resistance (R_{ct}) increases with PA concentration, the reason for which is that PA binds particularly to the imprinted polymer's pores, preventing $[Fe(CN)_6]^{3-/4-}$ from reaching the electrode surface, thus raising the resistance. Additionally, the logarithm of the PA concentration is proportional to the increase in the impedance response signal (R_{ct}). As illustrated in Figure 6B, when the PA concentration is between 10 pM to 100 µM, the calibration curve of MIP/GCE and lgC demonstrates a strong linear relationship, with a correlation coefficient of R^2 of 0.991. The detection limit for this compound can be calculated as 3.6 pM. The overall analytical performance of the MIP/GCE was compared with the previous literatures (see Table 1).

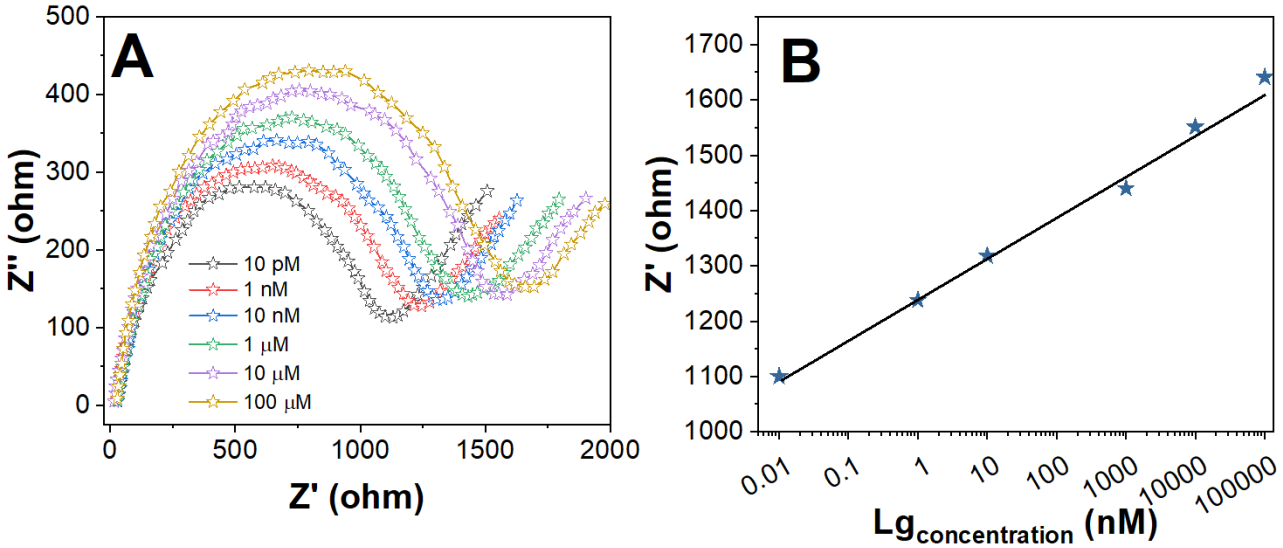

Figure 6. (A) EIS curves of the MIP/GCE towards 10 pM, 1 nM, 100 nM, 10 µM and 100 µM of PA. (B) The plot of logarithm of concentration v/s resistance.

Table 1. Comparison of MIP/GCE with previously reported PA sensors.

Electrode	Linear range	LOD	Reference
$Pt/CeO_2/Cu_2O$	0.5 µM to 100 µM	0.091 µM	[48]
MoS_2/TiO_2/GCE	0.5 µM to 750 µM	0.01 µM	[49]
N,S-doped Carbon@Pd Nanorods	33 nM to 120 µM	11 nM	[50]
FMWCNT/GCE	3 µM to 300 µM	0.6 µM	[51]
nano-Cu/GC_{EA}	4 µM to 12 µM	0.35 µM	[52]
PAMCPS	10 µM to 105 µM	53.37 nM	[53]
MIP/GCE	10 pM to 100 µM	3.6 pM	This work

The PA selectivity of MIP/GCE was determined with interfering compounds such as glucose (GLU), ascorbic acid (AA), aspirin (AS), ibuprofen (IB) and uric acid (UA). Figure 7 reveals the impedance response Rct of each compound in the electrochemical analysis. The greater the Rct value is, the more sensitive the sensor is to that material. To demonstrate that the molecularly imprinted sensor as constructed has a higher selectivity for PA molecules, the concentration of PA was set to 10 nM while the concentration of other molecules was adjusted to 100 nM. MIP/GCE had the greatest impedance response to the template molecule PA, but no apparent reaction occurred to the interference molecule. The reason for this phenomenon is the lack of specificity for other interfering chemicals in the MIPs.

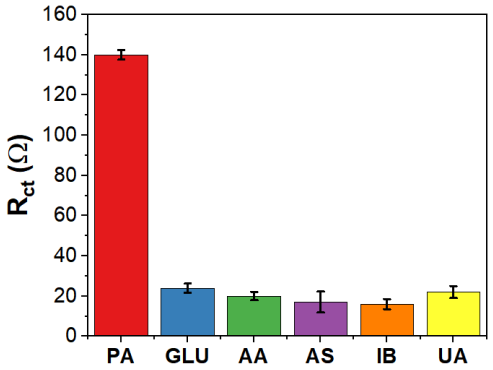

Figure 7. Response signals of PA and potential interfere species on MIP/GCE (n=3)

To exhibit the relevance of the proposed sensor for the detection of real sample (tablet) was analyzed. PA content of the sample was subjected to a standard addition method. The results were shown in Table 2. It shows that, the good recuperation of PA was observed in the range of 96.88% to 107.72%. This suggests the proposed method is relevant to the examination of medicinal samples in presence of different matrices.

Table 2. Real sample detection using MIP/GCE.

Sample	Found (µM)	Added (µM)	Found (µM)	Recovery (%)
Tablet 1	14.21	5.00	20.69	107.70
Tablet 2	19.51	10.00	28.89	97.90
Tablet 3	15.52	20.00	34.41	96.88

4. CONCLUSION

In this work, a particular detection approach for PA was established with molecular imprinting and electrochemical sensors. It was found that ethanol/acetic acid (V/V = 95:5) as eluent works best for 20 min. The impedance of the current increases with VAN concentration, the logarithm of the current

reduces with the increase of VAN concentration, from 1 pM to 0.1 mM, and the logarithm of the current drops linearly with the increase of PA concentration. However, the detection of PA in complex matrices cannot be conducted due to the low specificity of molecularly imprinted cavity recognition. Therefore, in future work, sensors with greater anti-interference capabilities need to be further explored to obtain more accurate detection of PA in the presence of many interfering chemicals.

References

1. L. Wang, Y. Yang, H. Liang, N. Wu, X. Peng, L. Wang, Y. Song, *J. Hazard. Mater.*, 409 (2021) 124528.
2. B.O. Orimolade, B.N. Zwane, B.A. Koiki, M. Rivallin, M. Bechelany, N. Mabuba, G. Lesage, M. Cretin, O.A. Arotiba, *J. Environ. Chem. Eng.*, 8 (2020) 104394.
3. N. Kumar, A.S. Bhadwal, B. Mizaikoff, S. Singh, C. Kranz, *Sens. Bio-Sens. Res.*, 24 (2019) 100288.
4. Y. Kumar, P. Pramanik, D.K. Das, *Heliyon*, 5 (2019) e02031.
5. Y. Yue, L. Su, M. Hao, W. Li, L. Zeng, S. Yan, *Front. Chem.*, 9 (2021) 479.
6. A. Kassa, M. Amare, *Cogent Chem.*, 5 (2019) 1681607.
7. R. Mangaiyarkarasi, S. Premlatha, R. Khan, R. Pratibha, S. Umadevi, *J. Mol. Liq.*, 319 (2020) 114255.
8. A. Pollap, K. Baran, N. Kuszewska, J. Kochana, *J. Electroanal. Chem.*, 878 (2020) 114574.
9. H. Karimi-Maleh, A. Khataee, F. Karimi, M. Baghayeri, L. Fu, J. Rouhi, C. Karaman, O. Karaman, R. Boukherroub, *Chemosphere* (2021) 132928.
10. M. Manjunatha Charithra, J.G. Manjunatha, *ChemistrySelect*, 5 (2020) 9323.
11. M.M. Charithra, J.G. Manjunatha, *J. Electrochem. Sci. Eng.*, 10 (2020) 29.
12. H. Karimi-Maleh, Y. Orooji, F. Karimi, M. Alizadeh, M. Baghayeri, J. Rouhi, S. Tajik, H. Beitollahi, S. Agarwal, V.K. Gupta, *Biosens. Bioelectron.* (2021) 113252.
13. Y. Zheng, D. Wang, X. Li, Z. Wang, Q. Zhou, L. Fu, Y. Yin, D. Creech, *Biosensors*, 11 (2021) 403.
14. D. Wang, D. Li, L. Fu, Y. Zheng, Y. Gu, F. Chen, S. Zhao, *Sensors*, 21 (2021) 8216.
15. M. Chen, H. Yang, Z. Song, Y. Gu, Y. Zheng, J. Zhu, A. Wang, L. Fu, *Phyton-Int. Exp. Bot.*, 90 (2021) 1507.
16. L. Fu, S. Mao, F. Chen, S. Zhao, W. Su, G. Lai, A. Yu, C.-T. Lin, *Chemosphere*, 297 (2022) 134127.
17. H. Karimi-Maleh, F. Karimi, L. Fu, A.L. Sanati, M. Alizadeh, C. Karaman, Y. Orooji, *J. Hazard. Mater.*, 423 (2022) 127058.
18. J. Liu, T. Yang, J. Xu, Y. Sun, *Front. Chem.*, 9 (2021) 488.
19. J. Lu, M. Cheng, C. Zhao, B. Li, H. Peng, Y. Zhang, Q. Shao, M. Hassan, *Ind. Crops Prod.*, 176 (2022) 114267.
20. A.S. Al-Gorair, M. Abdallah, *Int J Electrochem Sci*, 16 (2021) 210771.
21. S.A. Atty, A.H. Ibrahim, E.M. Hussien, *J. Electrochem. Soc.*, 166 (2019) B1483.
22. L. Fu, Y. Zheng, A. Wang, P. Zhang, S. Ding, W. Wu, Q. Zhou, F. Chen, S. Zhao, *J. Herb. Med.*, 30 (2021) 100512.
23. L. Fu, X. Zhang, S. Ding, F. Chen, Y. Lv, H. Zhang, S. Zhao, *Curr. Pharm. Anal.*, 18 (2022) 4–13.
24. H. Karimi-Maleh, C. Karaman, O. Karaman, F. Karimi, Y. Vasseghian, L. Fu, M. Baghayeri, J. Rouhi, P. Senthil Kumar, P.-L. Show, S. Rajendran, A.L. Sanati, A. Mirabi, *J. Nanostructure Chem.* (2022) in-press.

25. H. Karimi-Maleh, A. Ayati, S. Ghanbari, Y. Orooji, B. Tanhaei, F. Karimi, M. Alizadeh, J. Rouhi, L. Fu, M. Sillanpää, *J. Mol. Liq.*, 329 (2021) 115062.
26. M. Vinay, Y.A. Nayaka, *J. Sci. Adv. Mater. Devices*, 4 (2019) 442.
27. K. Kusuma, M. Manju, C. Ravikumar, H. Nagaswarupa, M.S. Amulya, M. Anilkumar, B. Avinash, K. Gurushantha, N. Ravikantha, *Sens. Int.*, 1 (2020) 100039.
28. T. Kokab, A. Shah, M.A. Khan, M. Arshad, J. Nisar, M.N. Ashiq, M.A. Zia, *ACS Appl. Nano Mater.*, 4 (2021) 4699.
29. K. Manjunatha, B.K. Swamy, H. Madhuchandra, K. Vishnumurthy, *Chem. Data Collect.*, 31 (2021) 100604.
30. J.R. Camargo, I.A. Andreotti, C. Kalinke, J.M. Henrique, J.A. Bonacin, B.C. Janegitz, *Talanta*, 208 (2020) 120458.
31. Md. Shalauddin, S. Akhter, W.J. Basirun, N.S. Anuar, O. Akbarzadeh, M.A. Mohammed, M.R. Johan, *Measurement*, 194 (2022) 110961.
32. M.S. Hussein, N. Al-Lami, O. H. R. Al-Jeilawi, *Chem. Methodol.*, 6 (2022) 319.
33. E. Nagles, M. Ceroni, J.J. Hurtado-Murillo, J.J. Hurtado, *Anal. Methods*, 12 (2020) 2608.
34. H. Beitollai, N. Arbabi, *Chem. Methodol.*, 6 (2022) 293–300.
35. W. Boumya, M. Achak, M. Bakasse, M. El Mhammedi, *J. Sci. Adv. Mater. Devices*, 5 (2020) 218.
36. A. Bozorgian, S. Zarinabadi, A. Samimi, *Chem. Methodol.*, 4 (2020) 477.
37. T.Y. Feyisa, S.A. Kitte, D. Yenealem, G. Gebretsadik, *Anal Bioanal Electrochem*, 12 (2020) 93.
38. M.H. Mohammed Al-Dahlaki, S. M.H. Al-Majidi, *Chem. Methodol.*, 6 (2022) 269.
39. A. K. Abass, A.K.M.A. Al-Sammarraie, *Chem. Methodol.*, 6 (2022) 301.
40. A.R. Maleki, L. Nateghi, P. Rajai, *Chem. Methodol.*, 6 (2022) 280.
41. A. Roy, B. Patnaik, I. Satpathy, *Eurasian Chem. Commun.* (2020) 991.
42. K. Harismah, M. Mirzaei, M. Da'i, Z. Roshandel, E. Salarrezaei, *Eurasian Chem. Commun.* (2021) 95.
43. M. Imran, S. Bokhary, S. Manzoor, M.K. Siddiqui, *Eurasian Chem. Commun.*, 2 (2020) 680.
44. M. Cancan, S. Ediz, M.R. Farahani, M. Farahani, *Eurasian Chem. Commun.*, 2 (2020) 641.
45. F. Afzal, M.A. Razaq, M.A. Razaq, D. Afzal, S. Hameed, *Eurasian Chem. Commun.*, 2 (2020) 652
46. F. Franceschini, M. Bartoli, A. Tagliaferro, S. Carrara, *Chemosensors*, 9 (2021) 361.
47. Y. Xu, Y. Lu, P. Zhang, Y. Wang, Y. Zheng, L. Fu, H. Zhang, C.-T. Lin, A. Yu, *Bioelectrochemistry*, 133 (2020) 107455.
48. A.R. Rajamani, S.C. Peter, *ACS Appl. Nano Mater.*, 1 (2018) 5148.
49. N. Kumar, A.S. Bhadwal, B. Mizaikoff, S. Singh, C. Kranz, *Sens. Bio-Sens. Res.*, 24 (2019) 100288.
50. L. Wang, Y. Yang, H. Liang, N. Wu, X. Peng, L. Wang, Y. Song, *J. Hazard. Mater.*, 409 (2021) 124528.
51. Z.A. Alothman, N. Bukhari, S.M. Wabaidur, S. Haider, *Sens. Actuators B Chem.*, 146 (2010) 314.
52. M.A. Kassem, M.I. Awad, M. Morad, B. Aljahdali, R.A. Pashameah, H. Alessa, G. Mohammed, A. Sayqal, *Int J Electrochem Sci*, 17 (2022) 220441.
53. M.M. Islam, M. Arifuzzaman, S. Rushd, M. Islam, M.M. Rahman, *Int J Electrochem Sci*, 17 (2022) 220230.